

Northumbria Research Link

Citation: Lai, Jintao, Yuan, Jinhui, Cheng, Yujun, Mei, Chao, Zhou, Xian, Wu, Qiang, Yan, Binbin, Wang, Kuiru, Long, Keping, Yu, Chongxiu and Sang, Xinzhu (2020) Dispersion-Engineered T-type Germanium Waveguide for Mid-Infrared Supercontinuum and Frequency Comb Generations in All-Normal Dispersion Region. OSA Continuum, 3 (9). pp. 2320-2331. ISSN 2578-7519

Published by: Optical Society of America

URL: <https://doi.org/10.1364/osac.399941> <<https://doi.org/10.1364/osac.399941>>

This version was downloaded from Northumbria Research Link:
<http://nrl.northumbria.ac.uk/id/eprint/44071/>

Northumbria University has developed Northumbria Research Link (NRL) to enable users to access the University's research output. Copyright © and moral rights for items on NRL are retained by the individual author(s) and/or other copyright owners. Single copies of full items can be reproduced, displayed or performed, and given to third parties in any format or medium for personal research or study, educational, or not-for-profit purposes without prior permission or charge, provided the authors, title and full bibliographic details are given, as well as a hyperlink and/or URL to the original metadata page. The content must not be changed in any way. Full items must not be sold commercially in any format or medium without formal permission of the copyright holder. The full policy is available online: <http://nrl.northumbria.ac.uk/policies.html>

This document may differ from the final, published version of the research and has been made available online in accordance with publisher policies. To read and/or cite from the published version of the research, please visit the publisher's website (a subscription may be required.)

Dispersion-Engineered T-type Germanium Waveguide for Mid-Infrared Supercontinuum and Frequency Comb Generations in All-Normal Dispersion Region

JINTAO LAI,¹ JINHUI YUAN,^{1,2,5} YUJUN CHENG,¹ CHAO MEI,² XIAN ZHOU,² QIANG WU,^{3,4,6} BINBIN YAN,¹ KUIRU WANG,¹ KEPING LONG,² CHONGXIU YU,¹ AND XINZHU SANG¹

¹State Key Laboratory of Information Photonics and Optical Communications, Beijing University of Posts and Telecommunications, Beijing 100876, China

²Research Center for Convergence Networks and Ubiquitous Services, University of Science & Technology Beijing, Beijing 100083, China

³Key Laboratory of Nondestructive Test (Ministry of Education), Nanchang Hangkong University, Nanchang 330063, China

⁴Department of Physics and Electrical Engineering, Northumbria University, Newcastle upon Tyne, NE1 8ST, United Kingdom

⁵yuanjinhui81@bupt.edu.cn

⁶qiang.wu@northumbria.ac.uk

Abstract: In this paper, a T-type Germanium (Ge) waveguide with the all-normal dispersion profile is designed for mid-infrared supercontinuum (SC) and frequency comb generations. The nonlinearity coefficient of the designed waveguide is calculated as $30.48 \text{ W}^{-1}\cdot\text{m}^{-1}$ at the initial pump wavelength of $3.0 \mu\text{m}$. Moreover, the group-velocity dispersion is kept low and flat in the considered wavelength range. Simulation results show that with the designed waveguide, the highly coherent and octave-spanning MIR SC can be generated in the wavelength range from 1.85 to $9.98 \mu\text{m}$ (more than 2.4 octaves) when the pump pulse with wavelength of $3.0 \mu\text{m}$, peak power of 900 W , and duration of 120 fs is launched into the 5 mm long waveguide. When the pulse train including 50 pulses at a repetition rate of 100 MHz is used as the pump source, the SC-based frequency comb is obtained.

© 2020 Optical Society of America under the terms of the [OSA Open Access Publishing Agreement](#)

1. Introduction

Mid-infrared (MIR) supercontinuum (SC) generation in optical waveguide has been extensively investigated in the field of nonlinear optics due to its potential applications in chip-scale optical frequency metrology, optical coherence tomography, nondestructive testing, bio-imaging and molecular spectroscopy [1–5]. The generation of the SC is resulted from the interaction of some nonlinear effects, which include self-phase modulation (SPM), optical wave breaking (OWB), stimulated Raman scattering (SRS), soliton fission (SF) [6, 7], etc.

The MIR SC generations in the traditional silicon (Si) waveguides have been attracting great research interests. In 2014, Ryan et al. firstly reported the octave-spanning SC generation in the wavelength range from 1.5 to $3.6 \mu\text{m}$ in the Si waveguide [8]. Since then, many works are concentrated on the MIR SC generations in the Si waveguides [9-13]. However, because the transparency window of the Si is limited to $8.5 \mu\text{m}$ [14], it is difficult to extend the SCs into the deep MIR region. In recent years, the germanium (Ge) as one of the group IV photonics materials becomes an excellent candidate material for the MIR SC generation since its optical characteristics are similar to the Si, while its transparency window ranges from 1.5 to $14.3 \mu\text{m}$, covering the “fingerprint” regions [14-16]. In 2015, Leonardis et

al. numerically investigated the nonlinear dynamics of the MIR SC generation in a Ge-on-Si strip waveguide [17]. In 2016, Yang et al. reported a low-dispersion Ge-on-Si waveguide for highly coherent SC generation from 3.7 to 9.24 μm [18]. In 2017, Yuan et al. proposed a suspended Ge membrane ridge waveguide, which can generate the SC spanning from 1.96 to 12 μm , extending deep into the “fingerprint” region [7]. In 2018, Sinobad et al. demonstrated an octave-spanning SC source in the Si-Ge waveguide, covering from 3 to 8.5 μm [19].

From the previous works [20-25], the dispersion has a crucial influence on the SC generation. When the pump pulse propagates in the anomalous dispersion region of the waveguide, the soliton dynamics dominate the nonlinear process of the SC generation [20-22]. Although the bandwidth of the generated SC can usually be up to the multiple octaves, the coherence of the SC can be greatly degraded by the noise amplification induced by modulation instability. In contrast, when the pump pulse propagates in the normal dispersion region of the waveguide, the SC has good coherence since the SPM and optical wave breaking (OWB) effects play important roles in the SC generation [23-25]. Moreover, the octave-spanning SC could also be generated through choosing the appropriate waveguide material and optimizing the waveguide structure. Meanwhile, by utilizing the highly coherent and octave-spanning SCs, the uniform and frequency stable optical frequency combs (OFCs) could be obtained. The SC-based OFCs have significant applications in high-performance atomic clock, high-precision optical frequency metrology, astronomical spectroscopy [26-29].

In this paper, we design a T-type Ge waveguide with all-normal dispersion profile. The influences of the pump pulse parameters, including center wavelength, peak power, and pulse duration on the SC generation are investigated by using the modified generalized nonlinear Schrödinger equation (GNLSE). Moreover, the nonlinear dynamics for the different waveguide lengths and noise coefficients are also demonstrated. Highly coherent and octave-spanning SCs are generated. Finally, the SC-based OFCs are obtained when a 50 pulses train at a repetition rate of 100 MHz is launched into the designed waveguide.

2. Theoretical model

The nonlinear dynamics of the SC generation in the Ge waveguide can be modelled by the modified GNLSE as following [17]

$$\frac{\partial A}{\partial z} + \frac{\alpha_0}{2} A - \sum_{m \geq 2} \frac{i^{m+1} \beta_m}{m!} \frac{\partial^m A}{\partial t^m} = i \left(\gamma + i \frac{\alpha_2}{2A_{\text{eff}}} \right) \times \left(1 + \tau_s \frac{\partial}{\partial t} \right) \times \left[A(z, t) \int_0^\infty R(t') |A(z, t-t')|^2 dt' \right], \quad (1)$$

where $A(z, t)$ is the slowly varying envelope, α_0 is the linear loss coefficient, β_m is the m -order dispersion coefficient calculated from Taylor expansion of the propagation constant, and α_2 is the two-photon absorption (TPA) coefficient. γ is the nonlinear coefficient, which can be described as

$$\gamma = \frac{2\pi n_2}{\lambda A_{\text{eff}}} = \frac{2\pi}{\lambda} \frac{\iint n_2(x, y) |\overline{F(x, y)}|^4 dx dy}{\left(\iint |\overline{F(x, y)}|^2 dx dy \right)^2}, \quad (2)$$

where $n_2(x, y)$ is the nonlinear refractive index, and $\overline{F(x, y)}$ represents the transverse distribution of the optical field [30].

The self-steepening $\tau_s = \gamma_1(\omega_0)/\gamma(\omega_0)$ and stimulated Raman scattering $R(t)$ are also considered. $\gamma_1(\omega) = d\gamma(\omega)/d\omega$, ω_0 is the central angular frequency, and $R(t)$ can be described as

$$R(t) = (1 - f_R) \delta(t) + f_R h_R(t), \quad (3)$$

where f_R is the fractional contribution of the Raman response. The delayed Raman response function $h_R(t)$ has the following form

$$h_R(t) = \frac{\tau_1^2 + \tau_2^2}{\tau_1 \tau_2^2} \exp\left(-\frac{t}{\tau_2}\right) \sin\left(\frac{t}{\tau_1}\right), \quad (4)$$

where $\tau_1 = 15.5 \times 10^{-15}$ and $\tau_2 = 230.5 \times 10^{-15}$ are the inverses of the phonon oscillation frequency and bandwidth of the Raman gain spectrum, respectively [31].

The degree of the first-order coherence $g_{12}^{(1)}$ of the SC is defined as

$$g_{12}^{(1)}(\lambda) = \frac{\langle E_1^*(\lambda) E_2(\lambda) \rangle}{\sqrt{\langle |E_1(\lambda)|^2 \rangle \langle |E_2(\lambda)|^2 \rangle}}, \quad (5)$$

where $E(\lambda)$ is the spectral amplitude of the generated SC in the frequency domain and can be obtained from the separate simulation with the different input noise. The noise can be described as

$$n = \eta \hat{N} \exp(i2\pi\hat{U}), \quad (6)$$

where η is the amplitude coefficient of the noise with respect to the input pulse, and \hat{N} and \hat{U} obey the standard normal and uniform distribution, respectively. In this work, we will perform 100 independent simulations and calculate the average over each pair of the output fields.

3. Design of the T-type Ge waveguide

Fig. 1(a) shows the three-dimensional structure of the designed T-type waveguide, where the waveguide structure is not drawn in scale and the core and substrate materials are Ge and silicon nitride (Si_3N_4), respectively. From Fig. 1(a), the T-type waveguide structure has a large refractive index contrast between the Ge and air, which is beneficial to the mode field confinement in the waveguide core. In order to provide the enough space between the Ge and Si_3N_4 layer, the height H_l and width W_l of the pillar are chosen as 1 and 0.3 μm , respectively. Fig. 1(b) shows the mode field distributions of the quasi-TE modes calculated at wavelengths 2, 4, 8, and 10 μm when the width W_u and height H_u of the membrane are chosen as 7 and 0.8 μm , respectively. It is worth indicating that compared with W_u and H_u , W_l has little effect on the mode field limitation. From Fig. 1(b), the mode fields of the quasi-TE modes can be well confined in the waveguide core even at wavelength 10 μm .

The group-velocity dispersion (GVD) of the designed waveguide can be derived from the effective refractive index of the guided mode [32]. In the following, we will investigate the influences of the geometric parameters of the waveguide including W_u and H_u on the dispersion characteristic. Fig. 2(a) shows the GVD coefficient β_2 for the quasi-TE mode as a function of wavelength when W_u remain unchanged and H_u increases from 0.7, to 0.8, to 0.9, and to 1.0 μm , respectively. From Fig. 2(a), as H_u increases, the curve of β_2 occurs to red-shift, and the value of β_2 decreases gradually. When $H_u=0.9$ μm , the curve of β_2 starts to move from the all-normal to anomalous dispersion region. In Fig. 2(b), when H_u remain unchanged and W_u decreases from 5, to 6, to 7, and to 8 μm , respectively, the curve of β_2 gradually moves from the all-normal to anomalous dispersion region. Thus, in order to achieve the all-normal dispersion, the optimized geometrical parameters of the T-type waveguide are chosen as $W_u = 7$ μm and $H_u = 0.8$ μm . It is worth indicating that H_l and W_l have little effect on β_2 . Fig. 3 shows the calculated β_2 and nonlinear coefficient γ as functions of wavelength for the quasi-TE mode when $W_u = 7$ μm and $H_u = 0.8$ μm . From Fig. 3, the all-normal dispersion is achieved in the considered wavelength range from 2 to 10 μm . Moreover, the variation of γ is monotonic, and its value can reach 30.48 $\text{W}^{-1}\cdot\text{m}^{-1}$ at the initial pump wavelength of 3.0 μm . In the following simulation, the 12-th order dispersions at wavelength 3.0 μm are considered, as shown in Table 1.

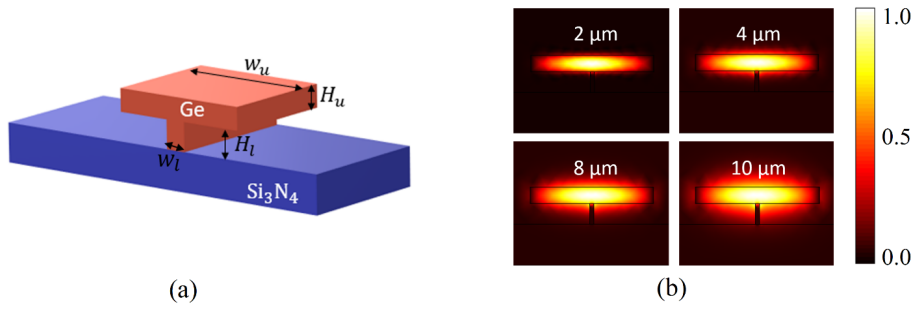


Fig. 1. (a) The three-dimensional structure of the proposed T-type Ge waveguide. (b) The mode field distributions of the quasi-TE modes when $W_u = 7 \mu\text{m}$, $H_u = 0.8 \mu\text{m}$, $H_l = 1.0 \mu\text{m}$, and $W_l = 0.3 \mu\text{m}$ at wavelengths 2, 4, 8, and 10 μm , respectively.

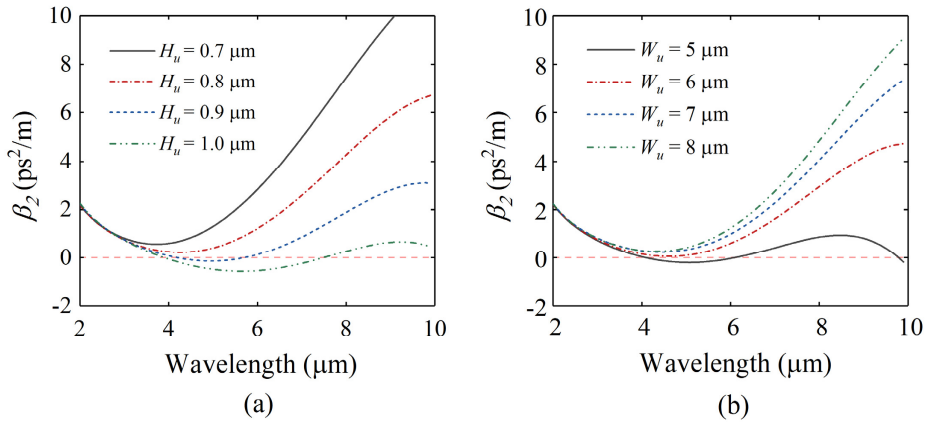


Fig. 2. The GVD coefficient β_2 of the quasi-TE mode calculated as a function of wavelength when (a) H_u and (b) W_u are changed, respectively.

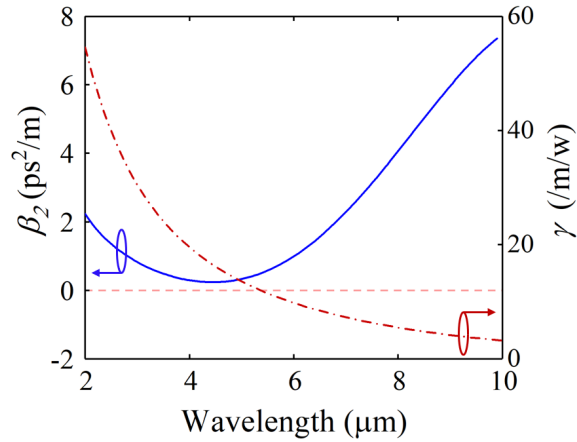


Fig. 3. The calculated β_2 and nonlinear coefficient γ as functions of wavelength when $W_u = 7 \mu\text{m}$ and $H_u = 0.8 \mu\text{m}$.

Table 1. The dispersion coefficient β_m calculated at wavelength 3.0 μm .

m	β_m
2	0.8178 ps ² /m
3	0.0040 ps ³ /m
4	1.0785 $\times 10^{-5}$ ps ⁴ /m
5	1.3559 $\times 10^{-9}$ ps ⁵ /m
6	-6.2852 $\times 10^{-9}$ ps ⁶ /m
7	-6.8421 $\times 10^{-11}$ ps ⁷ /m
8	6.0495 $\times 10^{-12}$ ps ⁸ /m
9	7.3555 $\times 10^{-14}$ ps ⁹ /m
10	-3.7414 $\times 10^{-15}$ ps ¹⁰ /m
11	-6.9163 $\times 10^{-17}$ ps ¹¹ /m
12	1.3735 $\times 10^{-18}$ ps ¹² /m

4. Simulation results and discussion

The nonlinear dynamics of the SC generation in the designed T-type Ge waveguide will be investigated by solving Eq. (1) with the Runge-Kutta algorithm. In the simulation, $\alpha_0 = 2$ dB/cm [7], $f_R = 0.076$ [33], and $n_2 = 44.03 \text{ is}^{-18} \text{ m}^2/\text{W}$ [10]. The nonlinear loss can be neglected because the TPA coefficient α_2 of the Ge material is equal to 0 when the pump wavelength is located at 3.0 μm . We will investigate the influences of the pump pulse parameters including the center wavelength, peak power, and pulse duration on the SC generation.

A linearly polarized hyperbolic secant pump pulse without chirp is launched into the proposed T-type Ge waveguide, whose geometrical parameters are chosen as $W_u = 7 \mu\text{m}$, $H_u = 0.8 \mu\text{m}$, $H_l = 1.0 \mu\text{m}$, and $W_l = 0.3 \mu\text{m}$. Figs. 4(a) and 4(b) show the temporal and spectral profiles of the generated SC after a propagation of 5 mm when the center wavelength of the pump pulse with the peak power of 900 W and duration of 120 fs is changed from 3.0, to 3.5, to 4.0, and to 4.5 μm , respectively. The nonlinear process is dominated by the combined effect of the dispersion and nonlinearity. Since the pump pulse works in the all-normal dispersion region of the waveguide, the spectral broadening is mainly resulted from the dispersion, SPM and OWB effects. From Fig. 4(a), many small oscillations caused by the long propagation distance can be observed at wavelength 3.0 μm . As the center wavelength of the pump pulse is changed from 3.0 to 4.5 μm , the pulse duration becomes narrower, and small oscillations gradually disappear. From Fig. 4(b), as the center wavelength of the pump pulse increases, the short wavelength side of optical spectrum occurs to red-shift, and its

bandwidth becomes smaller. The main reason for the decreasing bandwidth is considered that the dispersion and nonlinearity effects are weakened by the reduction of β_2 and γ as the center wavelength increases. When the center wavelength is located at 3.0 μm , the -40 dB bandwidth of the SC generated spans from 1.85 to 9.98 μm (more than 2.4 octaves). Fig. 4(c) shows the calculated first-order degree coherence $g_{12}^{(1)}$ of the generated SC. From Fig. 4(c), $g_{12}^{(1)}$ is maintained 1 in the considered wavelength range, which indicates that the SCs generated have good coherence.

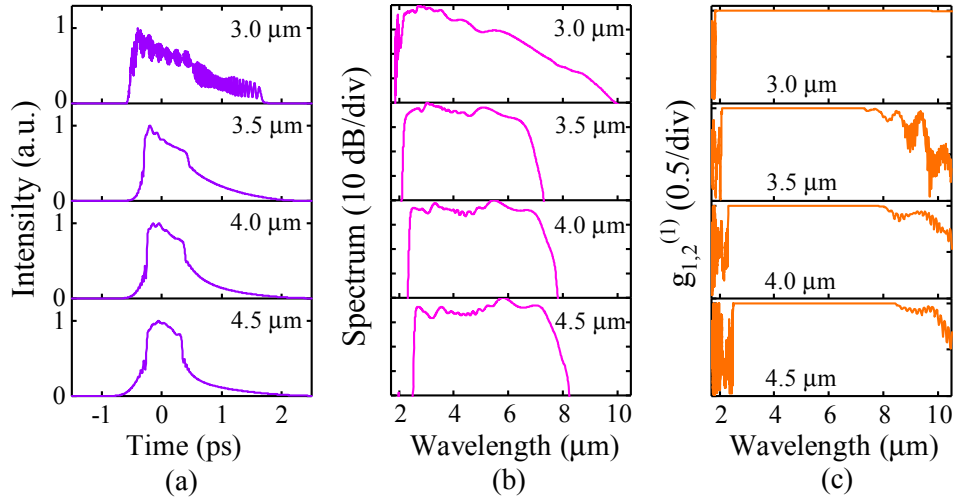


Fig. 4. (a), (b), and (c) show the temporal and spectral profiles and first-order degree coherence $g_{12}^{(1)}$ of the generated SC at the output end of the designed waveguide when the center wavelength of the pump pulse with the peak power of 900 W and duration of 120 fs is changed from 3.0, to 3.5, to 4.0, and to 4.5 μm , respectively.

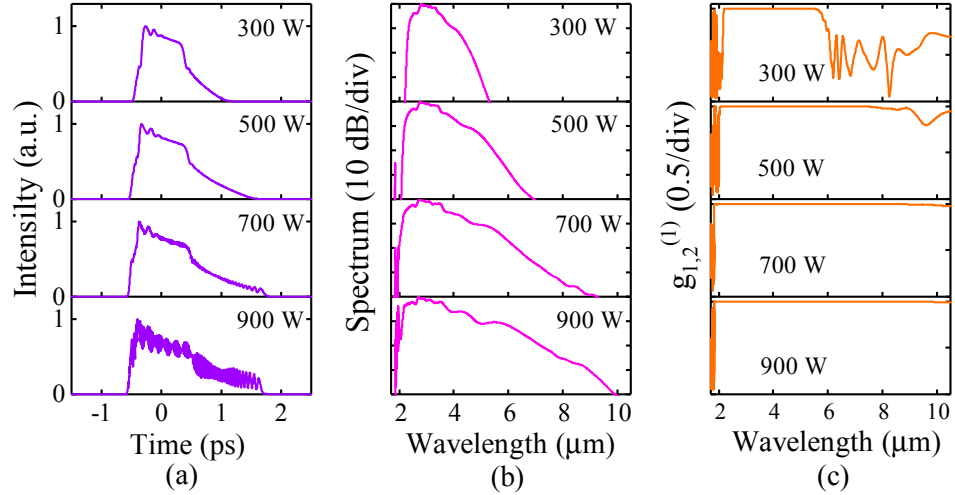


Fig. 5 (a), (b), and (c) show the temporal and spectral profiles and $g_{12}^{(1)}$ of the generated SC at the output end of the designed waveguide when the peak power of the pump pulse with the center wavelength of 3.0 μm and duration of 120 fs is changed from 300, to 500, to 700, and to 900 W, respectively.

Figs. 5(a) and 5(b) show the temporal and spectral profiles of the generated SC when the hyperbolic secant pump pulses with the center wavelength of 3.0 μm , duration of 120 fs, and peak power of 300, 500, 700, and 900 W are launched into a 5 mm long waveguide. From Fig. 5(a), as the peak power of the pump pulse is changed from 300 to 900 W, the pulse duration becomes wider, and some small oscillations emerge especially for the peak power of 900 W. From Fig. 5(b), the optical spectrum is broadened obviously as the peak power of the pump pulse is increased from 300 to 900 W. The main reason is considered that the SPM effect is enhanced by the increase of the peak power. When peak power is increased to 900 W, the -40 dB bandwidth of the SC generated is more than 2.4 octaves, spanning from 1.85 to 9.98 μm . Fig. 5(c) shows the calculated $g_{12}^{(1)}$ of the generated SC. From Fig. 5(c), $g_{12}^{(1)}$ is maintained 1, indicating good coherence of the SCs generated in the considered wavelength range. It is considered that the spectral width has exceeded 2.4 octaves and the kilowatt level peak power might be easy to damage the waveguide. Therefore, in the following investigation, we choose 900 W as the optimized peak power of the pump pulse.

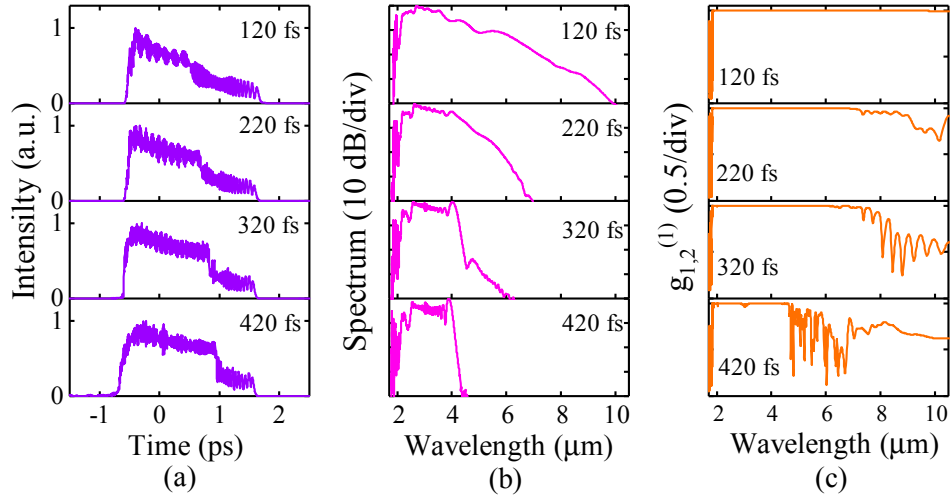


Fig. 6. (a), (b), and (c) show the temporal and spectral profiles and $g_{12}^{(1)}$ of the generated SC at the output end of the designed waveguide when the duration of the pump pulse with the center wavelength of 3.0 μm and peak power of 900 W is changed from 120, to 220, to 320, and to 420 fs, respectively.

Figs. 6(a) and 6(b) show the temporal and spectral profiles at the output end of the 5 mm long waveguide when the duration of the hyperbolic secant pump pulses with the center wavelength of 3.0 μm and peak power of 900 W is changed from 120 to 420 fs. From Fig. 6(a), as the duration of the pump pulse increases from 120 to 420 fs, many small oscillations are observed, and the pulse duration has no significant change. From Fig. 6(b), the bandwidth of the SC is decreased obviously, and the multi-peak oscillations appear as the duration of the pump pulse is increased. This is mainly induced by the decreased pulse energy and enhanced higher-order dispersion. Fig. 6(c) shows the calculated $g_{12}^{(1)}$ of the generated SC. It can be seen from Fig. 6(c) that the SCs generated in the considered wavelength range have good coherence. It is considered that a sufficiently wide spectral broadening can be achieved when the pulse duration is equal to 120 fs and the pulse duration of less than 100 fs is difficult to obtain. Therefore, the optimized pulse duration is chosen as 120 fs.

In summary, a 120 fs hyperbolic secant pulse with the center wavelength of 3.0 μm and peak power of 900 W can be used as the pump source. In the following, we will investigate

the influence of the waveguide length on the SC generation. When the waveguide length is changed from 2, to 5, to 8, and to 11 mm, the temporal and spectral profiles at the output end of the waveguide are shown in Figs. 7(a), 7(b), and 7(c), respectively. From Fig. 7(a), as the waveguide length is changed from 2 to 11 mm, the pulse duration gradually becomes wider, many small oscillations can be observed, and the intensity of small oscillations gradually becomes stronger. From Fig. 7(b), the spectral bandwidth is increased as the waveguide length is increased from 2 to 5 mm. However, when the waveguide length is increased to 8 and 11 mm, the spectral bandwidth doesn't expand further, and the spectral flatness starts to deteriorate. This is mainly because as the waveguide length increases, the OWB effect occurs due to the higher-order dispersion, and the spectral flatness becomes worse. In addition, the increasing propagation loss restricts the extension of the optical spectra. Fig. 7(c) shows the calculated $\mathcal{G}_{12}^{(1)}$ of the generated SC. It can be seen from Fig. 7(c) that the coherence of the generated SC can be still maintained good in the considered wavelength range even for the longer waveguide.

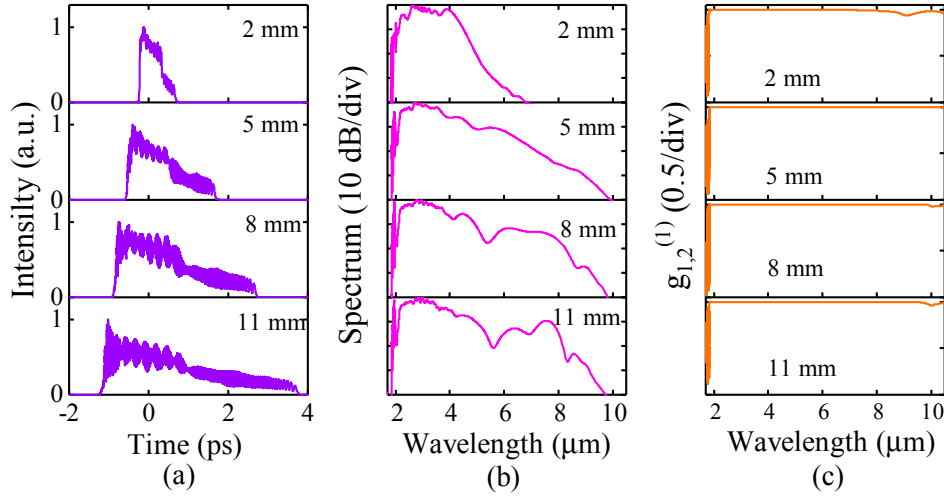


Fig. 7. (a), (b), and (c) show the temporal and spectral profiles and $\mathcal{G}_{12}^{(1)}$ of the generated SC at the output end of the designed waveguide when a 120 fs pulse with the center wavelength of 3.0 μm and peak power of 900 W is used as the pump source and the waveguide length is changed from 2, to 5, to 8, and to 11 mm, respectively.

Figs. 8(a) and 8(b) show the temporal and spectral profiles at the output end of the waveguide when η is chosen as 0, 0.001, 0.01, and 0.1, respectively. From Figs. 8(a) and 8(b), as η is increased from 0 to 0.1, many small oscillations with the increasing intensity emerge in the time domain, and the spectral fluctuation becomes evident gradually in the frequency domain. Fig. 8(c) shows the calculated $\mathcal{G}_{12}^{(1)}$ of the generated SC. From Fig. 8(c), when $\eta=0$ and 0.001, $\mathcal{G}_{12}^{(1)}$ is equal to 1 in the considered wavelength range, and the SCs generated have good coherence. In contrast, the coherence of the SC generated is degraded when $\eta=0.01$ and 0.1. Thus, good coherence of the SC generated can be obtained for the smaller η .

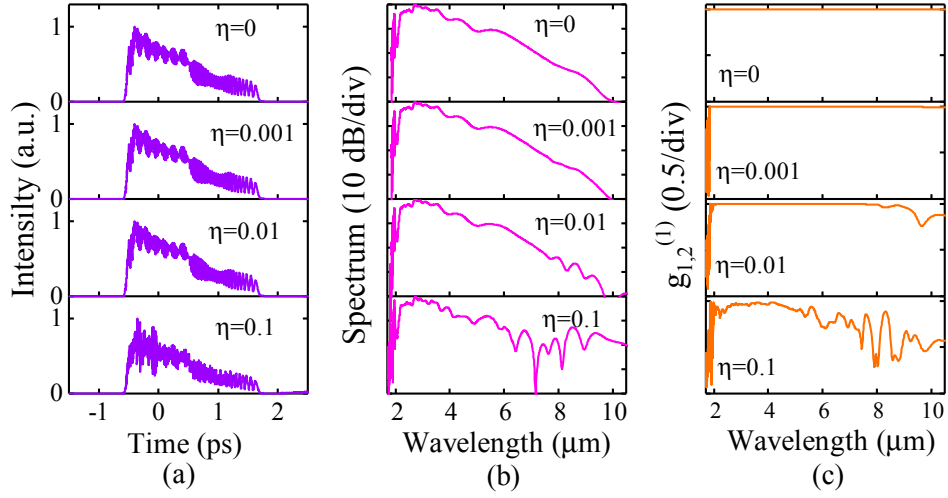


Fig. 8. (a), (b), and (c) show the temporal and spectral profiles and $g_{1,2}^{(1)}$ of the generated SC at the output end of the designed waveguide when a 120 fs pulse with the center wavelength of 3.0 μm and peak power of 900 W as the pump source is launched into the 5 mm long waveguide and η is changed from 0, to 0.001, to 0.01, and to 0.1, respectively.

Based on the above discussion, the highly coherent and octave-spanning MIR SC can be generated by optimizing the pump pulse parameters, waveguide length, and η . Figs. 9(a) and 9(b) show the temporal and spectral evolutions of the pump pulse when the hyperbolic secant pulse with wavelength of 3.0 μm , peak power of 900 W, and duration of 120 fs is used as the pump source, the waveguide length is chosen as 5 mm, and $\eta=0.001$. The corresponding temporal and spectral profiles at the input and output ends of the waveguide are also shown at the bottom and top of Figs. 9(a) and 9(b). From Fig. 9(a), the pulse is continuously extended, but its energy is always concentrated on the main peak during the propagation. And many small oscillations emerge at the output end of the waveguide. From Fig. 9(b), when the waveguide length is shorter than 1 mm, the optical spectrum is broadened symmetrically by the SPM effect. After the 1 mm length, the higher-order dispersion and OWB effects play important roles, and the optical spectrum gradually extends toward the longer wavelength. At the output end of the waveguide, the generated MIR SC spans from 1.85 to 9.98 μm at -40 dB level (more than 2.4 octaves), along with good coherence.

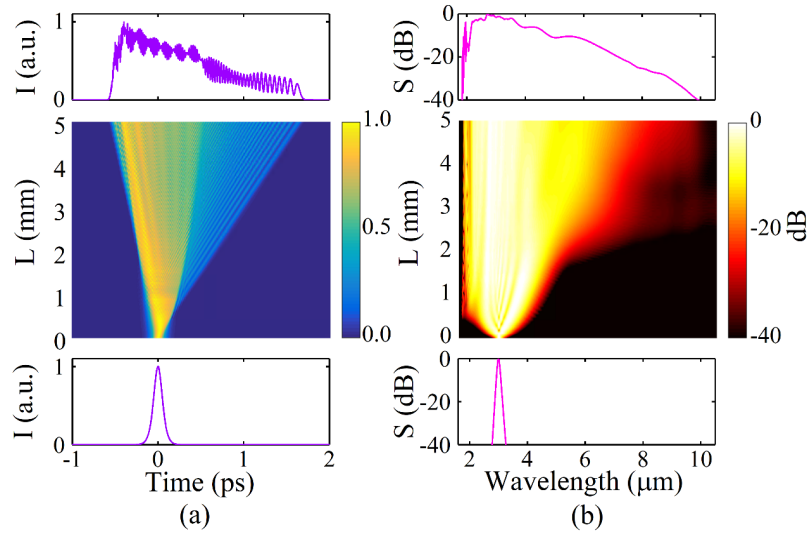


Fig. 9. (a) and (b) show the temporal and spectral evolutions along the waveguide length, the bottom and top figures showing the temporal and spectral profiles at the input and output ends of the waveguide. I in (a) represents the intensity. S in (b) represents the spectrum.

The SC-based frequency comb can be generated by launching a pump pulse train into the proposed waveguide. The pump pulse train includes 50 pulses and has a repetition rate of 100 MHz. Fig. 10(a) shows the generated SC-based frequency comb. To clearly show the comb line structure, Figs. 10(b) and 10(c) show the zoom-in views of the frequency comb generated at 50.03 THz/5.99 μm and 100.03 THz/2.99 μm with a sampling bandwidth of 500 MHz. It can be seen from Figs. 10(b) and 10(c) that in the sampling bandwidth of 500 MHz, the frequency intervals between each comb line are 100 MHz, and the amplitudes of the comb line in the sampling bandwidth are basically equal. It is worth indicating that the equal frequency interval of 100 MHz can be achieved in the considered spectral range from 0 to 180 THz. Thus, the frequency comb with stable amplitude and equal interval is obtained based on the highly coherent and octave-spanning MIR.SC generated in the designed waveguide.

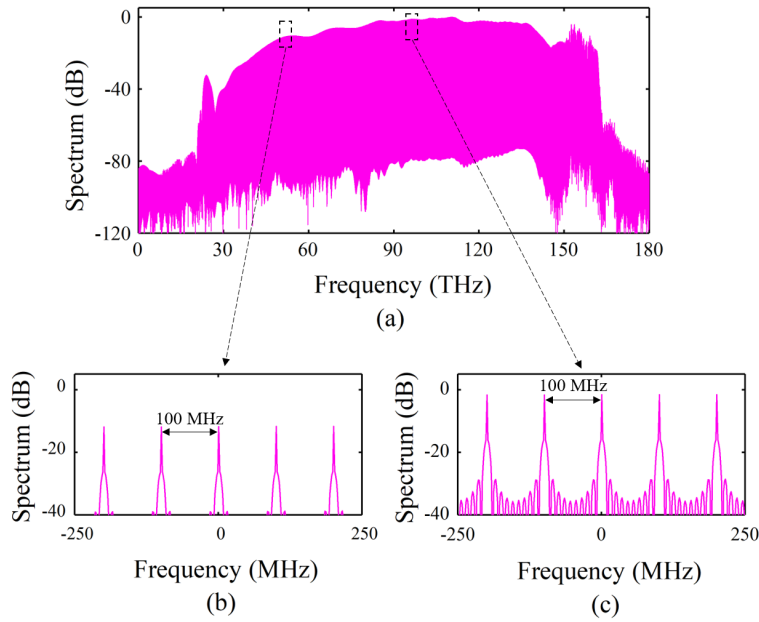


Fig. 10. (a) The SC-based frequency comb obtained with 50 input pulses at a repetition rate of 100 MHz. (b) and (c) The zoom-in views of the frequency comb generated at 50.03THz/5.99 μm and 100.03 THz/2.99 μm with a sampling bandwidth of 500 MHz.

At present, the plasma dry etching technology and atmospheric chemical vapor deposition technology can be used to fabricate the designed T-type Ge waveguide. The possible fabrication process of the designed waveguide is shown in Figs. 11(a)-11(d). First, with the atmospheric chemical vapor deposition technology [34], a Ge layer can be grown on the Si_3N_4 substrate [Fig. 11(a)]. Second, the traditional optical lithography with plasma reactive-ion dry etching is used to form a pillar [Fig. 11(b)]. Third, the Ge wafer is directly bonded onto the etched die by using the hydrophobic bonding technology [35,36] [Fig. 11(c)]. Finally, the final waveguide structure is formed [Fig. 11 (d)].

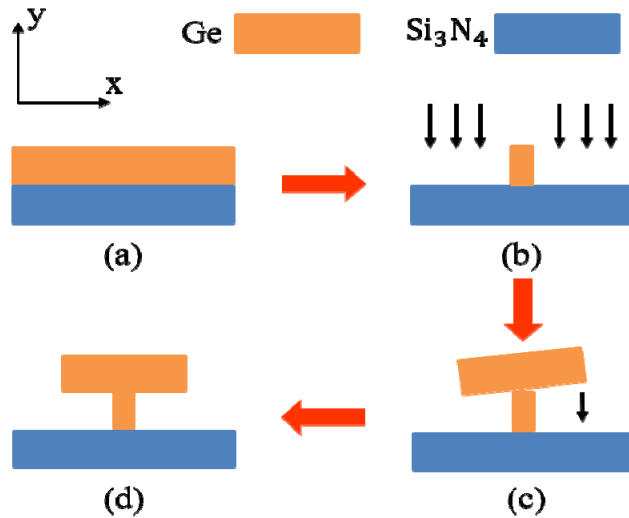


Fig. 11. The possible fabrication process flow: (a) deposition of Ge on Si_3N_4 substrate, (b) formation of the pillar, (c) Ge hydrophobic bonding, and (d) final waveguide structure.

5. Conclusions

In summary, we design a T-type Ge waveguide with the all-normal dispersion profile for the MIR SC and frequency comb generations. The influences of the pump pulse parameters, waveguide length, and noise coefficient on the SC generation are investigated. When the hyperbolic secant pump pulse with wavelength of 3.0 μm , peak power of 900 W, and duration of 120 fs is launched into the 5 mm long waveguide, the -40 dB bandwidth of the SC generated spans from 1.85 to 9.98 μm (more than 2.4 octaves). Moreover, the SC-based frequency comb is generated when a pump pulse train including 50 pulses at a repetition rate of 100 MHz is used. It is believed that our research results have important applications in biophotonics and spectroscopy, optical precision measurement, etc.

Acknowledgements

This work was supported by the National Natural Science Foundation of China (61875238).

Disclosures

The authors declare no conflicts of interest.

References

1. A. Schliesser, N. Picqué, and T. W. Hänsch, “Mid-infrared frequency combs,” *Nat. Photonics* **6**, 440–449 (2012).
2. H. Kano and H. O. Hamaguchi, “Vibrationally resonant imaging of a single living cell by supercontinuum-based multiplex coherent anti-Stokes Raman scattering microspectroscopy,” *Opt. Express* **13**(4), 1322–1327 (2005).
3. F. Keilmann, C. Gohle, and R. Holzwarth, “Time-domain mid-infrared frequency-comb spectrometer,” *Opt. Lett.* **29**(13), 1542–1544 (2004).
4. S. Dupont, C. Petersen, J. Thøgersen, C. Agger, O. Bang, and S. R. Keiding, “IR Microscopy utilizing intense supercontinuum light source,” *Opt. Express* **20**(5), 4887–4892 (2012).
5. C. S. Colley, J. C. Hebden, D. T. Delpy, A. D. Cambrey, R. A. Brown, E. A. Zibik, W. H. Ng, L. R. Wilson, and J. W. Cockburn, “Mid-infrared optical coherence tomography,” *Rev. Sci. Instrum.* **78**(12), 123108 (2007).
6. G. P. Agrawal, “Supercontinuum generation,” in *Nonlinear Fiber Optics*, 5th ed. 388–426 (Academic, 2013).
7. J. H. Yuan, Z. Kang, F. Li, et al., “Mid-infrared octave-spanning supercontinuum and frequency comb generation in a suspended germanium-membrane ridge waveguide,” *J. Lightwave Technol.* **35**, 2994–3002 (2017).
8. R. K. W. Lau, M. R. E. Lamont, A. G. Griffith, Y. Okawachi, M. Lipson, and A. L. Gaeta, “Octave-spanning mid-infrared supercontinuum generation in silicon nanowaveguides,” *Opt. Lett.* **39**, 4518–4521 (2014).
9. B. Kuyken et al., “An octave-spanning mid-infrared frequency comb generated in a silicon nanophotonic wire waveguide,” *Nat. Commun.* **6**, 6310 (2015).
10. L. Zhang, A. M. Agarwal, L. C. Kimerling and J. Michel, “Nonlinear Group IV photonics based on silicon and germanium: from near-infrared to mid-infrared,” *Nanophoton.* **3**(1), 247–268 (2014).
11. A. R. Johnson et al., “Octave-spanning coherent supercontinuum generation in a silicon nitride waveguide,” *Opt. Lett.* **40**(21), 5117–5120 (2015).
12. H. Saghaei, V. Van, “Broadband mid-infrared supercontinuum generation in dispersion-engineered silicon-on-insulator waveguide,” *JOSA* **36**(2), A193–A202 (2019).
13. N. Singh, D. D. Hudson, and B. J. Eggleton, “Silicon-on-sapphire pillar waveguides for Mid-IR supercontinuum generation,” *Opt. Express* **23**(13), 17345–17354 (2015).
14. R. Soref, “Mid-infrared photonics in silicon and germanium,” *Nat. Photon.* **4**, 495–497 (2010).
15. N. P. Barne and M. S. Piltch, “Temperature-dependent Sellmeier coefficients and nonlinear optics average power limit for germanium,” *J. Opt. Soc. Amer.* **69**(1), 178–180 (1979).
16. F. D. Leonardis, B. Troia, and V. M. N. Passaro, “Mid-IR optical and nonlinear properties of germanium on silicon optical waveguides,” *J. Lightw. Technol.* **32**(22), 3747–3757 (2014).
17. F. D. Leonardis, B. Troia, R. A. Soref, and V. M. N. Passaro, “Modelling of supercontinuum generation in the germanium-on-silicon waveguided platform,” *J. Lightw. Technol.* **33**(21), 4437–4444 (2015).
18. M. Yang, Y. Guo, J. Wang, et al. “Mid-infrared supercontinuum generation in a low-dispersion Ge-on-Si waveguide using sub-picosecond pulses,” *2016 IEEE 13th Intern. Conf. on Group IV Photonics (GFP)*. 36–37 (2016).
19. M. Sinobad, C. Monat, et al., “Mid-infrared octave spanning supercontinuum generation to 8.5 μm in silicon-germanium waveguides”. *Optica* **5**(4), 360–366 (2018)

20. Z. L. Li, J. H. Yuan, C. Mei, et al. "Multi-octave mid-infrared supercontinuum and frequency comb generation in a suspended As₂Se₃ ridge waveguide," *Appl. Opt.* **48**(31) 8404–8410 (2019).
21. M. R. Karim, H. Ahmad, S. Ghosh, and B. M. A. Rahman, "Design of dispersion-engineered As₂Se₃ channel waveguide for mid-infrared region supercontinuum generation," *J. Appl. Phys.* **123**(21), 213101 (2018).
22. M. R. Karim, B. M. Rahman, and G. P. Agrawal, "Mid-infrared supercontinuum generation using dispersion-engineered Ge_{11.5}As₂₄Se_{64.5} chalcogenide channel waveguide," *Opt. Express* **23**, 6903–6914 (2015).
23. C. Finot, B. Kibler, L. Provost, and S. Wabnitz, "Beneficial impact of wave-breaking or coherent continuum formation in normally dispersive nonlinear fibers," *J. Opt. Soc. Am. B* **25**, 1938–1948 (2008).
24. H. Ahmad, M. R. Karim, B. M. A. Rahman, "Modeling of dispersion engineered chalcogenide rib waveguide for ultraflat mid-infrared supercontinuum generation in all-normal dispersion regime," *Appl. Phys. B* **124**(3), 47 (2018).
25. T. S. Saini, N. P. T. Hoa, K. Nagasaka, X. Luo, T. H. Tuan, T. Suzuki, and Y. Ohishi, "Coherent mid-infrared supercontinuum generation using rib waveguide pumped with 200 fs laser pulses at 2.8 μm," *Appl. Opt.* **57**, 1689–1693 (2018).
26. A. Bartels, D. Heinecke, "10-GHz Self-Referenced Optical Frequency Comb," *Science* **326**(5953), 681–681 (2009).
27. M. T. Murphy, Th. Udem, R. Holzwarth, et al., "High-precision wavelength calibration of astronomical spectrographs with laser frequency combs," *Mon. Not. R. Astron. Soc.* **380**, 839–847 (2007).
28. C. H. Li, A. J. Benedick, P. Fendel, et al., "A laser frequency comb that enables radial velocity measurements with a precision of 1 cm s⁻¹," *Nature* **452**, 610–612 (2008).
29. T. Steinmetz, T. Wilken, C. Araujo-Hauck, et al., "Laser frequency combs for astronomical observations," *Science* **321**, 1335–1337 (2008).
30. J. Hu, C.R. Menyuk, L.B. Shaw, "Computational study of 3–5μm source created by using supercontinuum generation in As₂S₃ chalcogenide fibers with a pump at 2μm," *Opt. Lett.* **35**, 2907–2909 (2010).
31. L. Liu, T.L. Cheng, K. Nagasaka, H.T. Tong, T.B. Suzuki, Y. Ohishi, "Coherent mid-infrared supercontinuum generation in all solid chalcogenide micro-structured fibers with all-normal dispersion," *Opt. Lett.* **41**, 392–395 (2016).
32. K. Saitoh, M. Koshiba, "Finite Element Beam Propagation Method with Perfectly Matched Layers for Anisotropic Optical Waveguides," *J. Lightw. Technol.* **19**(3), 405–413 (2001).
33. N. K. Hon, R. Soref, and B. Jalali, "The third-order nonlinear optical coefficients of Si, Ge, and Si_{1-x}Ge_x in the midwave and longwave infrared," *J. Appl. Phys.* **110**(1), 1–8 (2011).
34. R. Loo, G. Wanga, L. Souriaua, J.C. Linc, S. Takeuchia, G. Brammertza, M. Caymaxa, "High quality Ge virtual substrates on Si wafers with standard STI patterning," *J. Electrochem. Soc.* **157**, H13–H21 (2010).
35. J. Chiles, S. Khan, J. C. Ma, and S. Fathpour, "High-contrast, all-silicon waveguiding platform for ultra-broadband mid-infrared photonics," *Appl. Phys. Lett.* **103**(15), 1–3 (2013).
36. S. Y. Ke, J. R. Zhou, D. L. Huang, et al., "Polycrystalline Ge intermediate layer for Ge/Si wafer bonding and defect elimination in Si (SOI)-based exfoliated Ge film," *Vacuum* **172**, 109047 (2020).